Sensors and Materials, Vol. 35, No. 8 (2023) 2983–3001
MYU Tokyo

S & M 3369

Analysis of "Fingerprint" Characteristics of Wireless Channels of Sensors in Mobile Communications

Songhua Hu,[1] Chunhao Yang,[1] Zuwei Hu,[1]
Mingxian Liu,[2] Zhenwei Wang,[3*] and Shi Yin[4]

[1]Baoshan Power Supply Bureau, Yunnan Power Grid Co., Ltd., Baoshan 678008, China
[2]Lijiang Power Supply Bureau, Yunnan Power Grid Co., Ltd., Lijiang 674100, China
[3]School of Aeronautics and Astronautics, Dalian University of Technology, Dalian 116024, China
[4]Faculty of Civil Aviation and Aeronautics, Kunming University of Science and Technology, Kunming 650500, China

(Received April 18, 2022; accepted August 10, 2023)

Keywords: channel modelling, singular value decomposition, Doppler extension, time delay extension, channel identification

The fingerprint feature analysis of wireless channels of sensors in mobile communications is the basis to support the application of sensors in mobile communication technology. In this paper, we propose a set of analytical research methods including the modeling, feature analysis, and scene identification of wireless channels for the realization of different fading characteristics of signals when transmitted in different wireless channels. (1) According to the transmission process of a signal in a wireless channel, considering the effect of the signal by noise interference in the wireless channel, a global wireless channel signal transmission model that introduces time-varying nature is established. (2) We proposed a wavelet noise reduction method based on singular value decomposition to attenuate the interference effect of noisy signals on channel characterization. (3) We proposed a method for extracting wireless channel features from the perspectives of Doppler expansion, time delay expansion, path loss, path gain, and signal peak analysis, and extracted wireless channel "fingerprint" features under three different scenarios through simulation analysis. (4) Finally, we established a fingerprint feature evaluation model on the basis of weight assignment and verified the feasibility of this evaluation model through example analysis. In this paper, we focused on the systematic research and analysis of the wireless channel features of sensors. The overall research idea still needs a large number of tests for verification, but it can provide an important reference for research on channel feature extraction.

1. Introduction

The Industry 4.0 era is a process of digitalizing industrial development based on technologies such as the Internet of Things, mobile communications, and digital twins. The new industrialization and marketization model brought about by the Industry 4.0 era is based on the

*Corresponding author: e-mail: 876382540@qq.com
https://doi.org/10.18494/SAM4516

ISSN 0914-4935
https://myukk.org/

integration of a large number of communication systems in tandem,[1,2] and therefore, there is an increasing demand for mobile communication technologies in this era. In mobile communication technology, the analysis of the signal transmission characteristics of wireless channels is crucial, and the key to this is in the analysis models of the "fingerprint" characteristics of wireless channels. The so-called fingerprint characteristics of wireless channels refer to the different performance characteristics of wireless signals in the propagation process in different scenarios and environments, and the different fading characteristics of signals in the propagation process can effectively reflect these different performance characteristics.

Currently, wireless channel characterization is a hot research field. Shi *et al.* established a dynamic wireless channel for power equipment storage scenarios in the context of power equipment storage.[3] Huang *et al.*[4] and Zhang *et al.*[5] studied the modeling of optical wireless channels for underwater environments.[4,5] Ranchagoda *et al.* proposed a two-ray average path loss model for A2G channels on the basis of the characteristics of the path loss of signals during propagation.[6] Many studies considered the effect of multipath fading during signal propagation in the analysis of wireless channel characteristics.[7–9] Hamdan *et al.* analyzed Rayleigh random channels with different Doppler diffusions from a rapidly varying level of flat fading.[10] In some other studies, a neural-network-based approach was used for the identification of wireless channel features.[11,12] From the above literature, it can be seen that current research methods for the characteristics of wireless channels are numerous and research scenarios are extensive, but there are problems, for example, the established mathematical models are not clearly described, signal characteristics are not collected comprehensively, and there is a lack of a systematic discussion from channel modeling and channel feature analysis to channel scene identification. In this paper, we first establish a clear signal transmission model of wireless channels, consider time-varying parameters, and establish a global wireless channel signal transmission model with the introduction of time-varying characteristics. Then, we extract the fingerprint features of the channels from the perspective of multiple channel features for a noise-reduced processed signal. Finally, we perform the scene recognition of an example using the established fingerprint feature evaluation model based on weight assignment.

2. Wireless Channel Modeling

2.1 Signal transmission model via wireless channels

The transmission process of the established wireless channel transmission model is shown in Fig. 1. After the output signal is set to be transmitted from the signal source at a certain moment, it enters the wireless channel through the transmission filter, and then there is a multipath delay that causes interference to the transmitted signal as the same transmitted signal takes different times to reach the receiver via each path. In addition, the multipath factor is introduced in this paper to describe the differences in the transmission paths of the transmitted signal in the wireless channel, i.e., each path has a different effect on the transmitted signal. The transmission of the transmitted signal in the wireless channel can also be affected by the external environment and introduce noise signal interference. The signal after the interference is transmitted to the

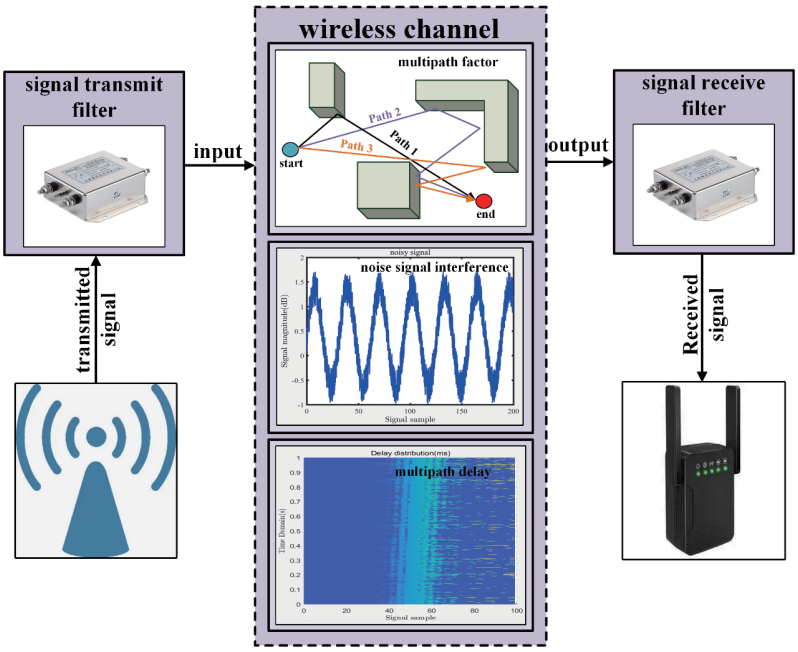

Fig. 1. (Color online) Signal transmission via wireless channels.

receiving device via a signal reception filter to obtain the measurement results of the transmitted signal, and the noise signal presented in this paper refers to any interference signal that may exist in the wireless channel of the test scenario.

On the basis of the above principles, the signal transmission via wireless channels is modeled as follows:

$$h[k]=\sum_{l=0}^{L-1} h_l \cdot \delta\left[k-\tau_l\right], k=0,1,\cdots,K-1, K \geq \max_l\left\{\tau_l\right\}, \tag{1}$$

$$r[k]=\sum_{m=0}^{M-1} h[k-m]\cdot g[m]+u[k], k=0,1,\cdots,K-1. \tag{2}$$

The channel sample points are distributed in the channel according to a certain time interval. If the sampling time interval is denoted as $\Delta\kappa$, then the sampling time interval $\Delta\kappa$ can be calculated as the total length of the signal, T_N, divided by the total number of samples, K. The signal sample points are sampled from the moment 0, and thus the channel sample point k is the code for the signal value collected at the moment $(k-1)\Delta\kappa$. In Eq. (1), L is the total number of signaling paths at the current time, h_l is the channel coefficient of the current l signaling path at the current time, $h[k]$ is the measurement result of the sample point k in the ideal channel, and τ_l is the signal delay of the current l signaling path at the current time, which is in integer multiples of the number of sample points. In Eq. (2), M is the filter length, $g[m]$ is the filter coefficient corresponding to the current filter length, which is equivalent to the effect of all filters in the wireless channel, $\sum_{m=0}^{M-1} h[k-m]\cdot g[m]$ is the effect of the filter on the ideal channel measurement,

and $u[k]$ is the effect of the noise signal introduced by the sample point k at that moment. In this paper, the unit pulse signal is used as the transmitted signal, and thus the transmitted signal is

$$\delta[k]=\begin{cases}0, & k\neq 0\\ 1. & k=0\end{cases} \tag{3}$$

2.2 Introduction of a time-varying global wireless channel signal transmission model

From the model established in Sect. 2.1, and considering that the parameters of wireless channels are susceptible to multiple factors in different environments, and therefore, there is time variability in the parameters, the signal transmission model of the global wireless channel after considering the time variability according to the theory of the flat fading channel model is as follows:

$$r[k,n]=\sum_{m=0}^{M-1} h[k-m,n]\cdot g[m]+u[k,n], k=0,1,\cdots,K-1, n=0,1,\cdots,N-1, \tag{4}$$

$$h[k,n]=\sum_{i=0}^{L-1} h_l[n]\cdot\delta\left[k-\tau_l[n]\right]. \tag{5}$$

In the above equation, n is the test moment corresponding to the sample identification point, N is the total number of samples at the test moment within the total test time, $r[k, n]$, $u[k, n]$, and $h[k, n]$ are the received signal at the sample identification point of k at the n test moment, the superimposed effect of the introduced noise, and the ideal new measurement result, respectively, $h_l[n]$ is the channel coefficient of the signaling path of l at the n test moment, and $\tau_l[n]$ is the signal delay of the signaling path of l at the n test moment. The signal transmission model of the global wireless channel with the introduction of time variability is three-dimensional, which can be described as the signal model shown in Fig. 2.

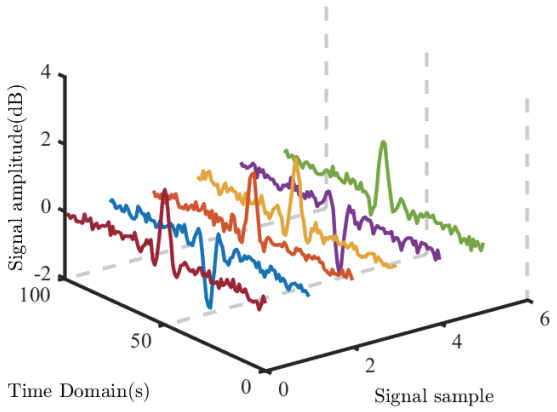

Fig. 2. (Color online) Three-dimensional signal transmission model.

3. Noise Reduction for Wireless Channel Models

For the noisy signal, the most widespread processing method is the threshold wavelet noise reduction method used in seismic data analysis,[13] medical field,[14,15] mechanical fault diagnosis,[16] and other aspects of noise reduction applications, which show significant results. This method mainly uses the Mallat algorithm for the wavelet analysis of the signal, using the characteristics of small noise wavelet coefficients, by setting *a suitable threshold*. In this study, we adopted the idea of wavelet noise reduction combined with singular value decomposition (SVD) and proposed a wavelet noise reduction method based on SVD, which can have a certain effect on reducing the Gaussian noise signal and can reduce the interference effect of the Gaussian noise signal on the transmitting signal for the subsequent simulation analysis, as shown in Fig. 3.

In the flow chart shown in Fig. 3, the key lies in the matrix construction and SVD of the signal containing Gaussian noise. From the wireless channel signal transmission model established in the previous section, it is known that at a certain time, the noisy signal can be expressed as $r[k]$, and the $r[k]$ matrix is constructed as a $K \times (K - L + 1)$ matrix where L takes (0.3–0.5)K and is a positive integer, so as to obtain the constructed noisy matrix as follows:

$$X = \begin{pmatrix} r[0] & r[1] & \cdots & r[K-L] \\ r[1] & r[2] & \cdots & r[K-L+1] \\ \vdots & \vdots & \ddots & \vdots \\ r[L-1] & r[L] & \cdots & r[K-1] \end{pmatrix}. \tag{6}$$

On the basis of the principle of SVD, the expression for the SVD of the noisy matrix can be obtained as

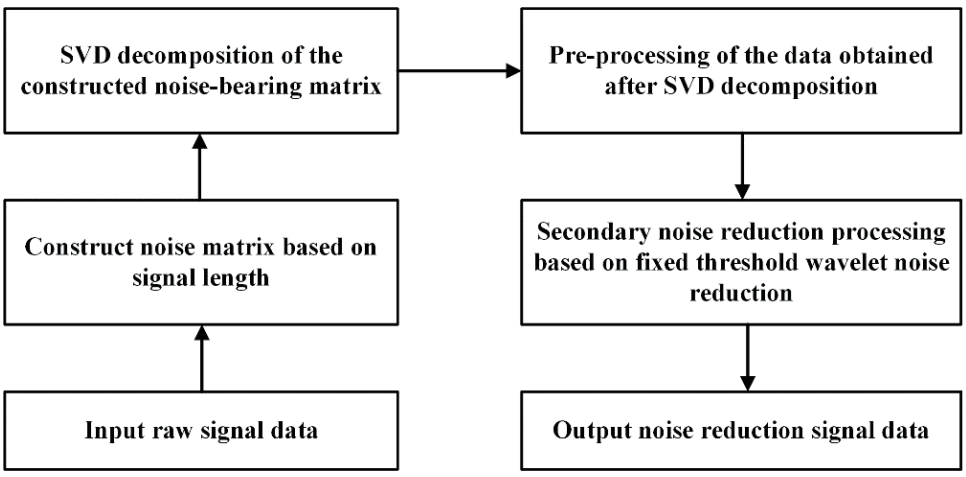

Fig. 3. Wavelet noise reduction based on SVD.

$$X = U \cdot \Sigma \cdot V^T. \tag{7}$$

In Eq. (8), U and V are the orthogonal matrices of $K \times K$ and $(K - L + 1) \times (K - L + 1)$, respectively, and Σ is the diagonal matrix of $K \times (K - L + 1)$ with non-negative diagonal elements in descending order. Thus, the matrices U, V, and Σ satisfy the following relations:

$$\begin{cases} U \cdot U^T = I, \\ V \cdot V^T = I, \\ \Sigma = diag\left(\sigma_1, \sigma_2, \cdots, \sigma_p\right), \\ \sigma_1 \geq \sigma_2 \geq \cdots \geq \sigma_p \geq 0, \\ p = \min(K, K - L + 1). \end{cases} \tag{8}$$

By using Eqs. (7) and (8), the SVD of the noisy matrix X can be achieved to obtain the matrices U, V, and Σ. Moreover, the appropriate principal singular value S_{va} is selected, zero is assigned to the elements from the number of rows where the singular value S_{va} in the matrix Σ is located to row $(N - \varepsilon + 1)$, and the matrix Σ' is obtained. After that, the preprocessing matrix can be obtained according to the equation $X' = U \cdot \Sigma' \cdot V^T$. The newly obtained matrix X' is the $K \times (K - L + 1)$ matrix, and the corresponding elements in the preprocessing matrix are extracted to obtain the preprocessing signal.

Furthermore, employing wavelet noise reduction to reduce noise in preprocessing signal is pursued. The specific procedure is outlined in Fig. 4. The specific process of wavelet noise reduction is to first decompose the original signal wavelet by selecting the appropriate wavelet type and the number of decomposition layers, obtaining each layer coefficient, and then setting a certain threshold for each layer coefficient for threshold processing. The threshold setting method here is selected according to a fixed threshold setting. The purpose of selecting the threshold is to reject the strong noise signal in the signal, because the SVD singular value can only carry out a certain noise reduction effect on the weak but persistent Gaussian signal in the environment. The effect on the strong noise signal in the environment is not obvious, so it is necessary to carry out secondary noise reduction treatment through wavelet noise reduction and denoise the layer coefficient according to the soft threshold denoising method. Finally, for the

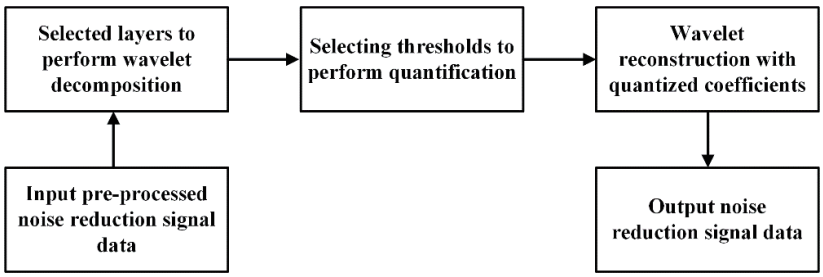

Fig. 4. Fixed-threshold-based wavelet noise reduction process flow.

processed layer coefficient (that is, the quantized coefficient), wavelet reconstruction is carried out to denoise the signal, so the core lies in the setting of the fixed threshold, which is set as

$$\lambda = \sqrt{2 \log N}. \tag{9}$$

After the above noise reduction, the denoised signal can be obtained as $r'[k]$. Therefore, on the basis of the above method, the signal sequence of each test moment can be noise-reduced in turn, and the global noise reduction signal can be obtained as $r'[k, n]$. It is worth mentioning that the denoising method proposed in this paper, based on SVD, has a certain attenuation effect on Gaussian noise interference within the noisy signal. However, it may not effectively reduce the strong interference caused by noise signals.

4. Fingerprint Feature Extraction for Wireless Channels

4.1 Fading characteristics of wireless channels

The signal propagation in wireless channels is affected by multipath transmission, that is, the signal in the scattering process occurs in the emission and diffraction phenomena, because in these phenomena, the wireless signal energy experiences a certain loss, resulting in rapid signal fluctuations at small-scale intervals. This nature of rapid fading during the propagation of signals over wireless channels is called small-scale fading or fast fading. In different environments, under different meteorological conditions, the small-scale fading superposition at each small-scale interval will cause the signal to change slowly at the macroscopic angle. The nature of this slow fading in the process of signal propagation in wireless channels is called large-scale fading or fast fading. This paper is based on the small- and large-scale fading characteristics of wireless channels, the extraction of the "fingerprint" characteristics of wireless channels, the commonly used path loss and path gain, the shadow effect to describe the large-scale fading of wireless signals, Doppler extension, and latency expansion to describe the small-scale fading of wireless channels.

With the small- and large-scale fading of wireless channels, the analysis of the shadow effect becomes tedious owing to the complex unknown nature of the scene environment and terrain. Thus, in this study, we used Doppler expansion, time delay expansion, and path loss to detect the fingerprint characteristics of wireless channels. In addition, to describe the fingerprint characteristics of wireless channels in more detail, time and frequency domain peak analyses were introduced in the simulation.

4.2 Basic parameters of signal data

To lay the foundation for the subsequent calculation of wireless channel feature parameters, the instantaneous amplitude and power of the signal need to be calculated and processed first. It is known that the signal after noise reduction is A, which is in the form of a complex signal, and the complex signal is specifically represented on the two-dimensional complex plane. To

simplify the effect of complex signals on the feature extraction of wireless channels, the complex signal is processed as follows in this paper:

$$A[k,n]=\begin{cases}\left|r'[k,n]\right|, & \text{if } real(r'[k,n])>0\vee(real(r'[k,n])=0\wedge imag(r'[k,n])<0)\\ -\left|r'[k,n]\right|, & \text{otherwise}\end{cases} \tag{10}$$

$$p[k,n]=\left(A[k,n]\right)^2, \tag{11}$$

$$A[k,n]\rightarrow \text{Fourier transform}\rightarrow Af[k,n]. \tag{12}$$

In Eq. (10), $A[k, n]$ is the instantaneous amplitude of the complex signal $r'[k, n]$, $real(r'[k, n])$ is the real part of the complex signal $r'[k, n]$, and $imag(r'[k, n])$ is the imaginary part of the complex signal $r'[k, n]$. In Eq. (11), $p[k, n]$ is the instantaneous power of the signal $r'[k, n]$, and Eq. (12) is the Fourier transform of $A[k, n]$ to obtain the data for the frequency domain analysis.

4.3 Characteristic parameters depicted

4.3.1 Doppler extension

Doppler extension is proposed on the basis of the Doppler effect of the signal, which arises owing to the nature of the frequency decay of the signal received when the receiving station is far away from the transmitting source, and in the Doppler effect, there is

$$f_m=\frac{v\cdot f_c}{c}. \tag{13}$$

In the above equation, f_m is the maximum frequency shift of the signal, f_c is the emission frequency of the signal, and c is the propagation speed of the electromagnetic wave under ideal conditions.

The Doppler expansion proposed in this paper is based on a typical Doppler power spectrum for analysis, described as

$$S(f)=\frac{1}{\pi\sqrt{{f_m}^2-(f-f_c)^2}},\left|f-f_c\right|<f_m. \tag{14}$$

In this paper, the Doppler power spectrum of the signal is presented on the basis of Eq. (14) in subsequent simulations, whereas the Doppler power value S_{f_0} at $f=f_c$ (when the frequency is the transmit frequency) in the Doppler power spectrum is used as a Doppler extension indicator to analyze the fingerprint characteristics of wireless channels.

4.3.2 Time delay extension

The temporal dispersion of wireless channels is analyzed on the basis of the distribution of the power delay profile (PDP). The parameters describing the time delay extension in the PDP are the average additional time delay $\overline{\tau}$ and the root-mean-square (rms) delay expansion σ_τ, calculated as

$$\overline{\tau} = \frac{\sum\limits_k a_k^2 \tau_k}{\sum\limits_k a_k^2} = \frac{\sum\limits_k P(\tau_k)\tau_k}{\sum\limits_k P(\tau_k)}, \tag{15}$$

$$\begin{cases} \sigma_\tau = \sqrt{E(\tau^2) - (\overline{\tau})^2}, \\ E(\tau^2) = \dfrac{\sum\limits_k a_k^2 \tau_k^2}{\sum\limits_k a_k^2} = \dfrac{\sum\limits_k P(\tau_k)\tau_k^2}{\sum\limits_k P(\tau_k)}. \end{cases} \tag{16}$$

In Eq. (15), a_k is the attenuation coefficient of the signal on the k path and $P(\tau_k)$ is the expected value of the received signal power in the τ_k time delay state on the k path. On the basis of the above equations, we propose a global average additional time delay and the global rms time delay expansion. These are also proposed on the basis of the global wireless channel signal transmission model with the introduction of time variability. First, the reference time τ_0 is determined on the basis of the power and time domain relationship of the step signal input to the filter in the ideal state. In the global wireless channel signal transmission model with the introduction of time variability, the test moment $n_{r'_{top}}$ and the corresponding power p at which each signal peak $r'_{top}[k,n]$ is located in the 3D signal data in the time domain analysis are extracted, and the time delay at each signal peak is the difference between the test moment n and the reference time τ_0. The signal peak data for which the difference is positive is extracted and calculated according to the following relationships:

$$\tau_0 = \frac{\sum\limits_k p_0[k] \cdot k \cdot \Delta t}{\sum\limits_k p_0[k]}, \tag{17}$$

$$\tau\left[k, n_{r'_{top}}\right] = n_{r'_{top}} \cdot \Delta t - \tau_0, \tag{18}$$

$$\overline{\tau}_{global} = \frac{\sum\limits_k \sum\limits_n p[k,n] \cdot \tau[k,n]}{\sum\limits_k \sum\limits_n p[k,n]}, \tag{19}$$

$$\begin{cases} \sigma_{global} = \sqrt{E\left(\tau_{global}^2\right) - \left(\overline{\tau}_{global}\right)^2}, \\ E\left(\tau_{global}^2\right) = \dfrac{\sum\limits_k \sum\limits_n p[k,n] \cdot \tau[k,n]}{\sum\limits_k \sum\limits_n p[k,n]}. \end{cases} \tag{20}$$

In the above equations, $p_0[k]$ is the instantaneous power of the step signal input to the filter at the signal identification point k, Δt is the measurement interval of adjacent samples in the signal sequence, $\tau[k, n_{r'_{top}}]$ is the time delay corresponding to the peak of the signal at $r'_{top}[k,n]$, $\overline{\tau}_{global}$ is the global additional time delay, σ_{global} is the global rms time delay expansion, and $E\left(\tau_{global}^2\right)$ is the expected value of the quadratic global additional delay. In this study, σ_{global} and $E\left(\tau_{global}^2\right)$ were used as the delay extensions in the fingerprinting of wireless channels, and the global delay map was plotted on the basis of $\tau[k, n_{r'_{top}}]$ in the simulation analysis to clearly demonstrate the global delay distribution.

4.3.3 Path loss and path gain

The path loss and path gain in wireless channels are properties used to describe the power changes of signals during transmission. In the propagation process of signals in wireless channels, the strong interference effects of noise signals in the channels are generally ignored. The power of the signal typically exhibits path loss due to the radiation and diffusion of the signal. Path loss is commonly expressed in decibels as the ratio of the transmitted signal power to the received signal power.

$$P_L \text{ dB} = 10 \log_{10} \frac{P_t}{P_r} \tag{21}$$

When $P_L > 0$, the signal power change is expressed as a path loss. When $P_L < 0$, the power variation of a signal exhibits a path gain. The main cause of the signal path gain is attributed to the strong interference effects of noise signals present in the testing scenario and the limited distance of the test, which leads to a less pronounced radiation and diffusion effect of the signal. In this study, the path loss of the signal was calculated in the subsequent simulation, the form of the variation of the signal power during the channel transmission was judged, the data was fitted using linear least squares, and the slope K_{PL} of the fitted straight line obtained was used as the characteristic index of the wireless channel.

4.3.4 Signal peak analysis

In this study, the signal amplitude peaks were extracted from the three-dimensional signal model from the perspective of time and frequency domain analyses. The numbers of signal amplitude peaks in different amplitude ranges in the time and frequency domain analyses were

counted at [α_1, α_2, α_3] and [β_1, β_2, β_3], and the sequence of the number of signal amplitude peaks in each amplitude range extracted was used as the peak analysis index of wireless channels.

5. Simulation Analysis

The simulation analysis in this study was carried out using Matlab R2017a software, and the signal data for conducting the simulation was based on the measurement results of a unit step signal provided by a technology company for the transmitted signal in three different scenarios. The total time of each test was 1 s, the total number of samples at the test moment in the total test time of each scenario was 1500, i.e., $N = 1500$, the measurement interval of the adjacent channel samples was 2/3 ms, the channel samples at each test moment contained 100 sample points, i.e., $K = 100$, and the measurement interval of adjacent samples in the signal sequence was $\Delta t = 65$ ns. The three sets of data corresponding to the above three scenarios were modeled in the three-dimensional coordinate system of the time domain, signal sample points, and signal real part amplitude, and subjected to least-squares fitting operation. The corresponding results are shown in Fig. 5.

5.1 Data preprocessing

On the basis of the noise reduction principle mentioned in Sect. 3, noise reduction was carried out for the three scenarios requiring channel characterization. The noise reduction results of $r'[k, 10]$, $r'[k, 100]$, $r'[k, 500]$, and $r'[k, 1000]$, and the corresponding signal sequences of the original signals in scene 1 are shown in Figs. 6(a)–6(d), respectively. The SVD-based wavelet noise reduction method has a certain effect on the elimination of Gaussian noise. Since the noise reduction part belongs to the signal processing part of this study and is not the core of this study, the noise reduction effect is not described in detail from the signal-to-noise ratio and other data.

After the wavelet noise reduction, the three-dimensional signal data were first analyzed in the time and frequency domains. On the basis of the calculation method proposed in the preceding work to find the instantaneous amplitude and power of the signal, the data $A[k, n]$ and

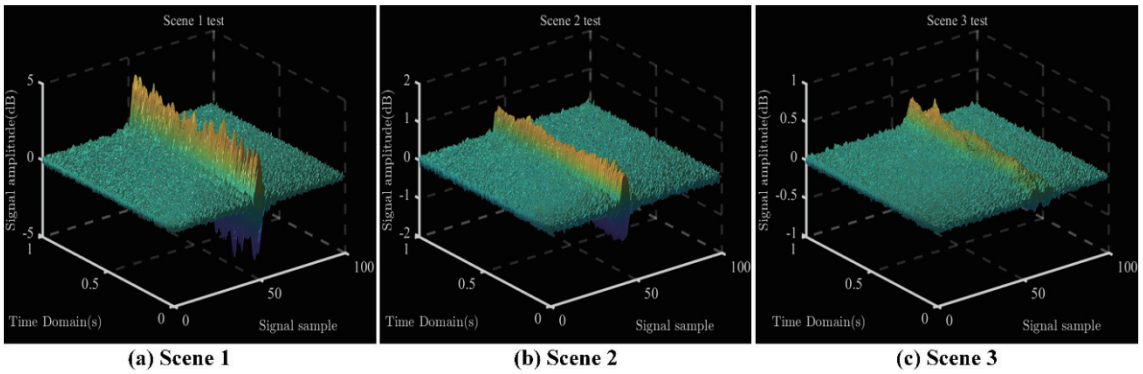

(a) Scene 1 **(b) Scene 2** **(c) Scene 3**

Fig. 5. (Color online) Presentation of 3D signal data in three scenarios.

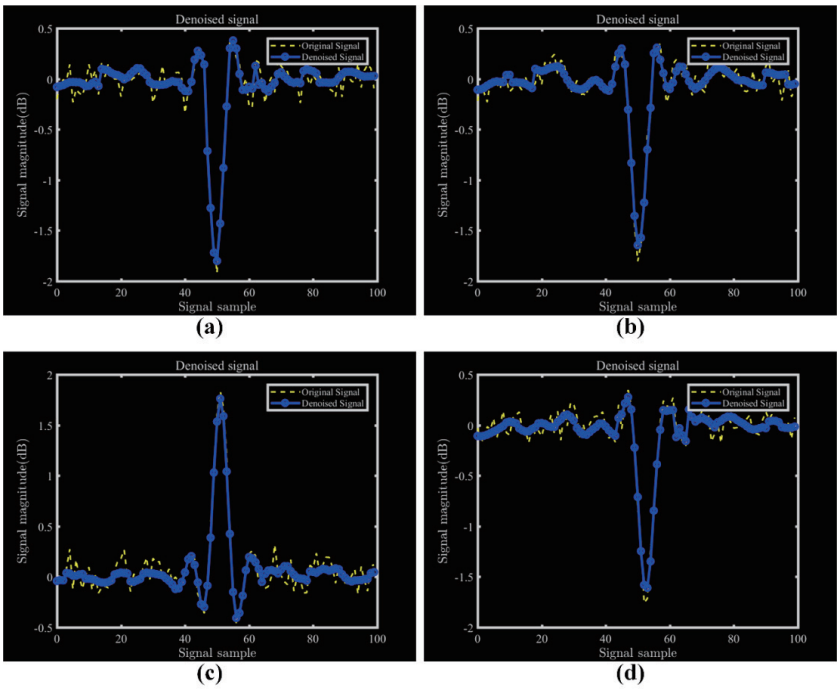

Fig. 6. (Color online) Noise reduction effect demonstration. (a) $r'[k, 10]$, (b) $r'[k, 10]$, (c) $r'[k, 10]$, and (d) $r'[k, 10]$.

$p[k, n]$ were obtained. Moreover, the data $Af[k, n]$ were obtained by Fourier transform, and the power $pf[k, n]$ corresponding to $Af[k, n]$ can be derived similarly according to Eq. (10). The frequency domain analysis results of the 3D signal data and the corresponding signal power spectra for the three scenarios are plotted in Fig. 7.

To analyze the time delay extension of wireless channels, it is necessary to first analyze the step signal input to the filter in an ideal state. According to the filter parameters provided by the technology company, the length of the filter is described as $M = 49$, and the power distribution obtained after inputting the unit step signal to this filter is shown in Fig. 8.

The calculation gives the base time $\tau_0 = 0.0017$ ms.

5.2 Fingerprint characterization of wireless channels

On the basis of the description of the characteristic parameters of wireless channels in the previous section, the path loss values obtained by linear least squares fitting are shown in Fig. 9, and typical Doppler power spectra and global delay distributions for the three scenarios were obtained as shown in Fig. 10.

As shown in Fig. 9, both Scenarios 1 and 3 exhibit path gain due to external noise environmental factors and the short test distance, but Scenario 1 reflects the phenomenon that the signal has less power change during propagation. The results of the time and frequency domain peak analyses for the three scenes are shown in Fig. 11. The time domain peak sequences $[\alpha_1, \alpha_2, \alpha_3]$ and $\alpha_1, \alpha_2, \alpha_3$ represent the numbers of signal peaks in the peak ranges of $[0.5, \infty)$,

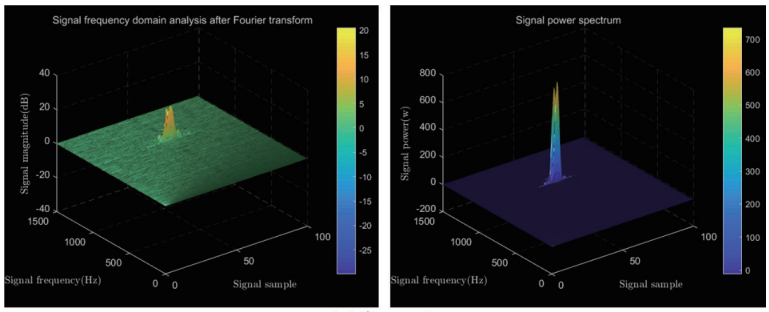

(a) Scene 1

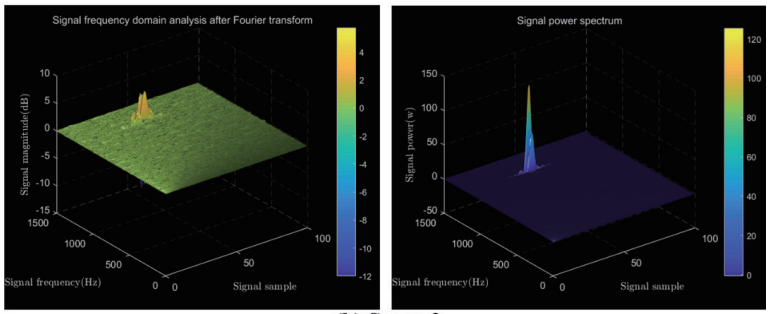

(b) Scene 2

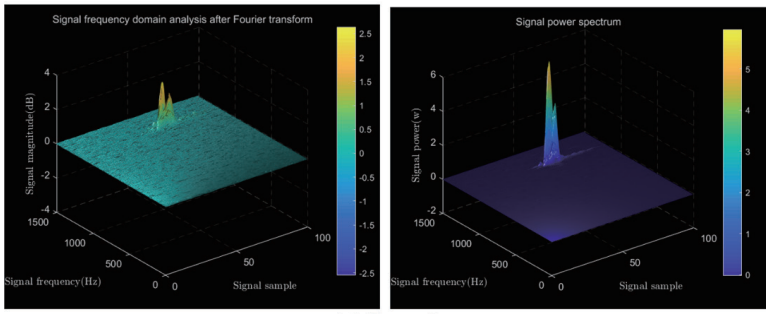

(c) Scene 3

Fig. 7. (Color online) Frequency domain analysis results (left) and power spectra (right) for three scenarios.

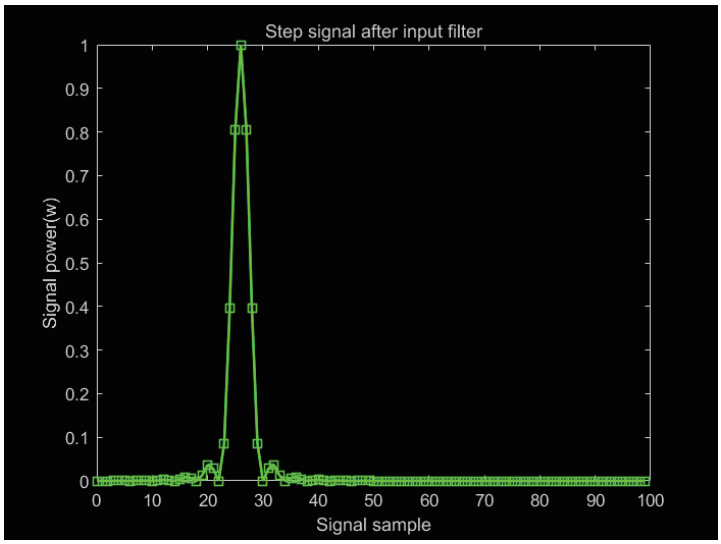

Fig. 8. (Color online) Unit step signal of input filter in ideal state.

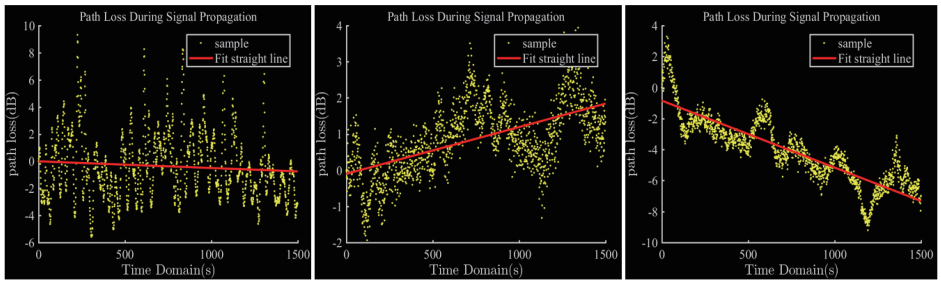

Fig. 9. (Color online) Sample and path loss values obtained by linear least squares fitting.

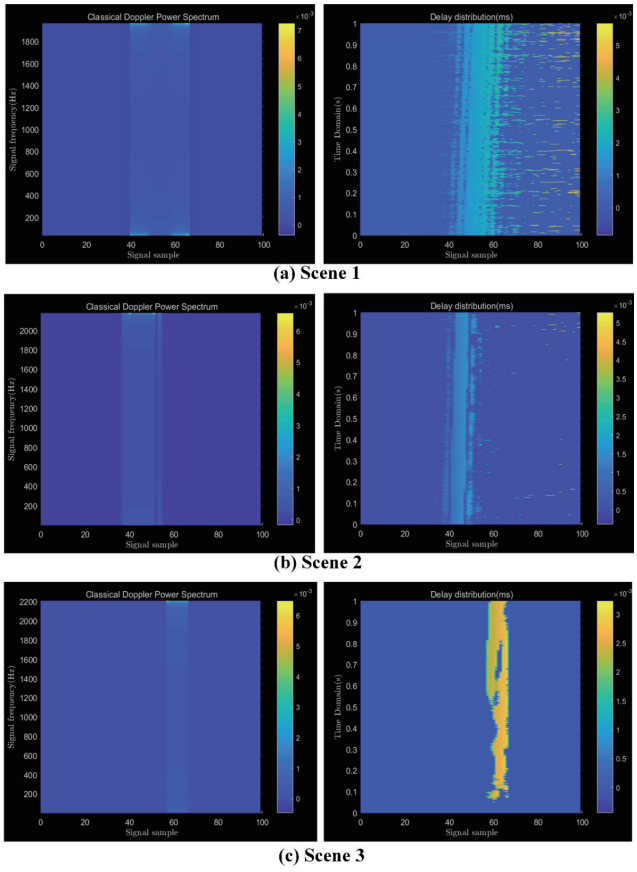

Fig. 10. (Color online) Doppler power spectra (left) and global time delay distributions (right).

[0.1, 0.5), and [0.05, 0.1), respectively, and the frequency domain peak sequence [β_1, β_2, β_3] represents the same range as [α_1, α_2, α_3].

According to the definition of each feature indicator in the previous section, the relevant feature indicators were calculated to obtain the relevant feature data shown in Table 1.

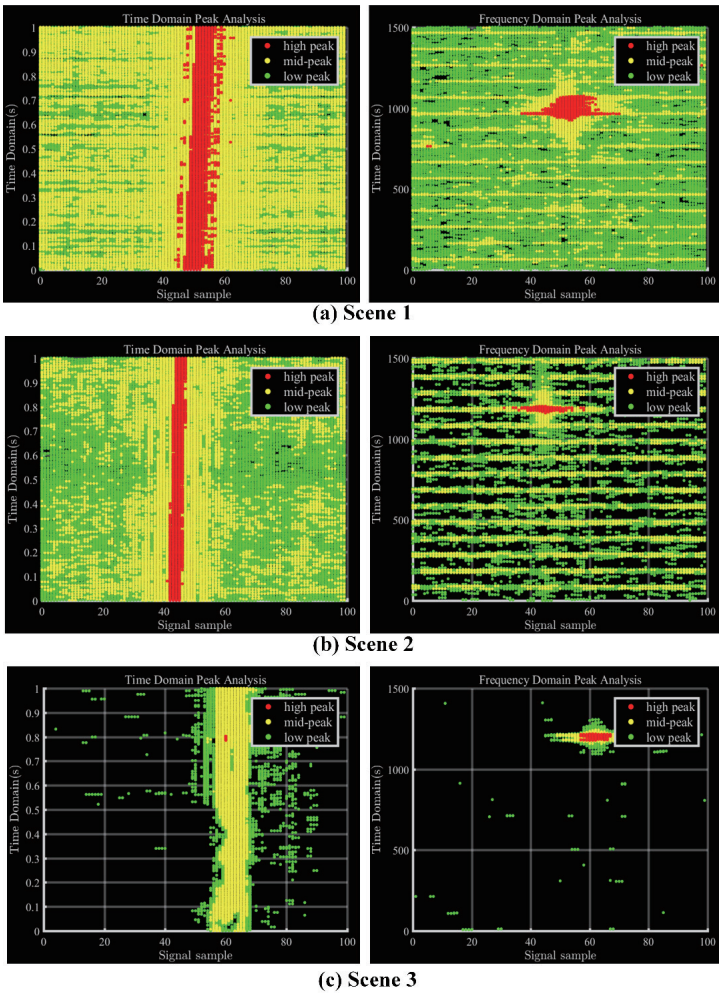

Fig. 11. (Color online) Results of time (left) and frequency (right) domain peak analyses.

Table 1
Summary of channel characterization data.

	Scene 1	Scene 2	Scene 3
Doppler extension indicators S_{f_0}	3.3×10^{-4}	2.7×10^{-4}	2.6×10^{-4}
Time delay scaling metrics $[\overline{\tau}_{global}, \sigma_{global}]$	$[1.7 \times 10^{-3}, 1.9 \times 10^{-4}]$	$[1.2 \times 10^{-3}, 1.5 \times 10^{-4}]$	$[2.3 \times 10^{-3}, 1.5 \times 10^{-4}]$
Path loss or path gain indicator K_{PL}	-4.9×10^{-4}	1.3×10^{-3}	-4.3×10^{-3}
Time domain peak analysis indicators $[\alpha_1, \alpha_2, \alpha_3]$	[9801, 40077, 50470]	[5374, 18712, 52273]	[21, 13006, 6989]
Frequency domain peak analysis metrics $[\beta_1, \beta_2, \beta_3]$	[1290, 10160, 40074]	[300, 6359, 17972]	[292, 776, 999]

6. Fingerprint Feature Scene Recognition

6.1 Fingerprint feature evaluation model based on weight assignment

In this study, on the basis of the obtained wireless channel fingerprint feature parameters of the known scenes, a weight assignment method is applied to construct a similarity matrix Z for scene identification, described as

$$z_{ij} = \sum_{n} \omega_n \cdot \delta_n \ (i \in judge, j \in scenes), \tag{22}$$

$$z_{ij} = \max\left\{z_{i1}, z_{i2}, \cdots, z_{ij}, \cdots\right\} \Rightarrow i = j. \tag{23}$$

In Eq. (22), δ_n is the similarity index of n, ω_n is the weight of the similarity index of n, which can be represented by the weight vector $\boldsymbol{\omega} = [\omega_1, \omega_2, ..., \omega_n]$, z_{ij} in the matrix Z is the similarity between the channel scene to be identified in i and the channel scene with known features in j, *judge* is the set of channel scenes to be identified, and *scenes* is the set of channel scenes with known features. Equation (23) is the decision for scene identification, i.e., the channel scene for which the largest item in the ith row of the likelihood matrix Z corresponds to a known feature is the channel scene to be identified.

For the similarity index, according to the Doppler expansion, time delay expansion, path loss, path gain, frequency domain peak analysis, and time domain peak analysis proposed in this paper, five similarity indexes can be calculated, as shown in Table 2.

Table 2
Calculated of similarity indexes.

Similarity index	Corresponding channel characteristics	Indicator calculation methodology
δ_1	Doppler extension	$1-\frac{\left\|S_{f_0}^i - S_{f_0}^j\right\|}{\max\left\{S_{f_0}^i, S_{f_0}^j\right\}}$
δ_2	Time delay extension	$1-\frac{\left\|\overline{\tau}_{global}^i - \overline{\tau}_{global}^j\right\|}{\max\left\{\overline{\tau}_{global}^i, \overline{\tau}_{global}^j\right\}} \cdot \frac{\left\|\sigma_{global}^i - \sigma_{global}^j\right\|}{\max\left\{\sigma_{global}^i, \sigma_{global}^j\right\}}$
δ_3	Path loss or path gain	$1-\frac{\arctan\left(K_{PL}^i\right) - \arctan\left(K_{PL}^j\right)}{\pi}$
δ_4	Time domain peak analysis	$1-\frac{1}{3}\sum_{k=1}^{3}\left\|\frac{\alpha_k^i}{\sum_{m=1}^{3}\alpha_m^i} - \frac{\alpha_k^j}{\sum_{m=1}^{3}\alpha_m^j}\right\|$
δ_5	Frequency domain peak analysis	$1-\frac{1}{3}\sum_{k=1}^{3}\left\|\frac{\beta_k^i}{\sum_{m=1}^{3}\beta_m^i} - \frac{\beta_k^j}{\sum_{m=1}^{3}\beta_m^j}\right\|$

6.2 Instance verification

In this study, the channel characteristics of the three different scenes extracted in the simulation analysis are the channel scenes with known characteristics, and the signal data based on the unit step signal as the transmitted signal in the three different scenes were measured again in the same way in the above three scenes, and the new three sets of data corresponding to the above three scenes were modeled in the three-dimensional coordinate system of the time domain, signal sample points, and signal amplitude, and subjected to noise reduction. The three-dimensional signal schematic obtained by the least squares fitting operation is shown in Fig. 12.

According to the fingerprint feature extraction method for wireless channels proposed in this paper to extract the feature parameters of wireless channels, the weight vector used was $\boldsymbol{\omega}$ = [0.15, 0.25, 0.2, 0.15, 0.25]. This weight vector was set manually after many trials, and the similarity index was calculated by combining the channel scenes with known features, and the similarity matrix was obtained as follows:

$$Z = \begin{pmatrix} 0.9908 & 0.9385 & 0.8806 \\ 0.9325 & 0.9893 & 0.9071 \\ 0.8953 & 0.9176 & 0.9712 \end{pmatrix}. \tag{24}$$

The above equation shows that the diagonal elements in the matrix Z are the maximum values. Thus, the identified scenes correctly correspond to the scenes to which they belong, which verifies the feasibility of the established fingerprint feature evaluation model based on weight assignment in scene identification.

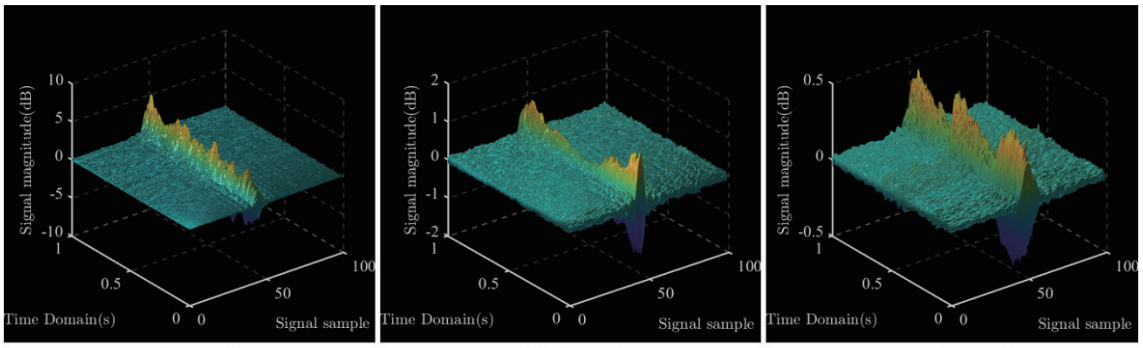

Fig. 12. (Color online) Remeasured 3D signal data in three scenarios.

7. Conclusions

In this paper, we first established a signal transmission model for wireless channels on the basis of the effects of multipath coefficients, multipath delay, and scene noise on the propagation of signals in wireless channels, and then we considered the effects of the time-varying parameters on the propagation of signals in wireless channels and established a global wireless channel signal transmission model with the introduction of time-varying parameters. To reduce the effect of the noise signal on the extraction of the fingerprint characteristics of wireless channels, we adopted a wavelet noise reduction method on the basis of SVD to reduce the noise of the signal data. The subsequent experiments demonstrated that the noise reduction method can reduce the effect of noise signals on the measurement data, but cannot eliminate the interference effect of strong noise signals on signal transmission. Moreover, we described the wireless channel characteristics in terms of signal Doppler expansion, time delay expansion, path loss, path gain, and peak analysis based on the small- and large-scale fading characteristics of the signal, and simulated and analyzed the measurement results under different scenarios. Finally, we established a fingerprint feature evaluation model on the basis of the weight assignment and verified the feasibility of the model in the scene identification of wireless channels after example analysis. Although the analysis of the fingerprint features of wireless channels in this study showed a certain degree of feasibility, it did not use a large amount of data for verification, and a large amount of measurement data is still needed to test the model, simulation analysis, and scene identification methods. However, the overall idea framework of wireless channel fingerprint analysis in this paper can provide an important practical reference for wireless communication, interconnection technology, signal analysis, and other fields.

Acknowledgments

This work was supported by the science and technology project of China Southern Power Grid Co., Ltd., which provided funding under project number YNKJXM20220216.

References

1 F. Zezulka, P. Marcon, I. Vesely, and O. Sajdl: IFAC-PapersOnLine **49** (2016) 8. https://doi.org/10.1016/j.ifacol.2016.12.002
2 X. Li, D. Li, J. Wan, A. V. Vasilakos, C. Lai, and S. Wang: Wireless Netw. **23** (2017) 23. https://doi.org/10.1007/s11276-015-1133-7
3 G. Shi, Y. He, B. Li, L. Zuo, B. Yin, W. Zeng, and F. Ali: Future Gener Comput Syst. **101** (2019) 492. https://doi.org/10.1016/j.future.2019.06.032
4 J. Huang, G. Wen, J. Dai, L. Zhang, and J. Wang: Opt. Commun. **473** (2020) 125989. https://doi.org/473.10.1016/j.optcom.2020.125989
5 J. Zhang, L. Kou, Y. Yang, F. He, and Z Duan: Opt. Commun. **475** (2020) 126214. https://doi.org/10.1016/j.optcom.2020.126214
6 N. H. Ranchagoda, K. Sithamparanathan, M. Ding, A. Al-Hourani, and K. M. Gomez: Veh. Commun. **32** (2021) 100393. https://doi.org/10.1016/j.vehcom.2021.100393
7 V. Lavanya, G. S. Rao, and B. Bidikar: Proc. Computer Science **85** (2016) 777. https://doi.org/10.1016/j.procs.2016.05.265
8 D. Manoranjan, S. Benudhar, and B. Urmila: Phys. Commun. **39** (2020) 101031. https://doi.org/39.10.1016/j.phycom.2020.101031

9 J. F. Blanza and L. Materum: J. Franklin Inst. **395** (2022) 2359. https://doi.org/10.1016/j.jfranklin.2022.01.007.
10 A. Hamdan, L. Ros, H. Hijazi, C. Siclet, and A. Al-Ghouwayel: Digit Signal Process. **117** (2021) 103189. https://doi.org/10.1016/j.dsp.2021.103189.
11 A. Ahangarzadeh, M. Hashemi, and S. A. Nezamalhosseini: Phys. Commun. **53** (2022) 101756. https://doi.org/10.1016/j.phycom.2022.101756
12 Y. Wan, Q. Lu, Y. Jin, and H. Zhang: J. Franklin Inst. **358** (2021) 6368. https://doi.org/10.1016/j.jfranklin.2021.06.013
13 F. Qin, J. Liu, Y. Cheng, and L. Lu: Research Square (2022). https://doi.org/10.21203/rs.3.rs-1866893/v1.
14 H. Khor, G. Ning, X. Zhang, and H. Liao: IEEE J Biomed Health Inform. **26** (2022) 3080. https://doi.org/10.1109/JBHI.2022.3144628.
15 K. Hanlon, G. Wei, J. Braue, L. Correa-Selm, and J. Grichnik: Lasers Surg Med. **64** (2021) 384. https://doi.org/10.1002/lsm.23483
16 N. Gharesi, M. M. Arefi, R. Razavi-Far, J. Zarei, and S. Yin: Adv. Eng. Inform. **46** (2020) 101172. https://doi.org/10.1016/j.aei.2020.101172

About the Authors

Songhua Hu was born in 1976 in Anning City, Yunnan Province. He graduated from Yunnan Electric Power School in 1996 and has been working as a first-class expert and senior technician in the substation operation of Baoshan Power Supply Bureau since 1996. His main research direction is the intelligent application of power system substations. (husonghua@bs.yn.csg.cn)

Zhenwei Wang was born in 2001 in Dalian, Liaoning Province, China. He received his bachelor's degree in mechanical engineering from Kunming University of Science and Technology in July 2023 and is currently pursuing a master's degree in aerospace science and technology from Dalian University of Technology. His main research interests are artificial intelligence, mobile communications, and aircraft control. (876382540@qq.com)